Sensors and Actuators B 176 (2013) 166–173

Contents lists available at SciVerse ScienceDirect

Sensors and Actuators B: Chemical

journal homepage: www.elsevier.com/locate/snb

NO_2 gas sensing with SnO_2–ZnO/PANI composite thick film fabricated from porous nanosolid

Hongyan Xu[a,b,*], Xingqiao Chen[c], Jun Zhang[a], Jieqiang Wang[a], Bingqiang Cao[a,b,*], Deliang Cui[d]

[a] School of Materials Science and Engineering, University of Jinan, Jinan 250022, PR China
[b] Shandong Provincial Key Laboratory of Preparation and Measurement of Building Materials, University of Jinan, Jinan 250022, PR China
[c] Shandong Swan Cotton Industrial Machinery Stock Co., Ltd., Jinan 250032, PR China
[d] State Key Laboratory of Crystal Material, Shandong University, Jinan 250100, PR China

ARTICLE INFO

Article history:
Received 5 April 2012
Received in revised form
14 September 2012
Accepted 19 September 2012
Available online xxx

Keywords:
SnO_2–ZnO porous nanosolid
Polyaniline
Composite
NO_2
Gas sensitivity

ABSTRACT

SnO_2–ZnO/polyaniline (PANI) composite thick film for NO_2 detection was fabricated from SnO_2–ZnO porous nanosolid and PANI by a conventional coating method. The SnO_2–ZnO composite porous nanosolid was prepared by a solvo-thermal hot-press (SHP) method. It was found that the composite sensor has high selectivity and response to low concentration NO_2 gas. Furthermore, the composite sensor also showed high stability to NO_2 over a long working period at low optimum working temperature (180 °C). The response and recovery times of SnO_2/PANI composite sensor (SZ20-P) were as short as about 9 and 27 s to 35 ppm NO_2 at 180 °C, respectively. The experiment results show that both the pore structures of SnO_2 porous nanosolid and the content of ZnO had effects on the sensor response of SnO_2–ZnO/PANI composites, and the optimum content of ZnO was 20 wt.%. The possible sensing mechanism was discussed.

1. Introduction

Nitrogen dioxide (NO_2) can be produced by many of processes like automobile exhaust fumes, production of nitric acid, the combustion of coal and fuel, etc. [1]. Nowadays, NO_2 is one of the hazardous gases polluting the atmosphere in urban areas. Moreover, the chemical reaction of NO_2 gas with water vapor would cause acid rain [2]. Therefore, the development of a NO_2 gas sensor for environmental monitoring has become a very important task.

Semiconducting tin oxide (SnO_2) has been proven to be one of the most attractive sensing materials for gas sensor applications, owing to its suitable physical–chemical properties, and possibility to detect many reducing and oxidizing gases with high response. However, the requirement of high operating temperature (>300 °C) is a major issue [3–6].

Recently, several organic semiconductors, such as polyaniline (PANI), polypyrrole (PPy), polythiophene (PTh) and metal substituted phthalocyanines (MSPs) have been used for detecting toxic gases (such as NO_2, O_3) [7–12]. As one kind of conducting polymers, PANI and its derivatives, have received considerable attention for their low working temperature, low cost, easy preparation, and thermal stability [13,14].

However, PANI still exhibits some shortcoming as gas sensitive materials, including low sensitivity, irreversible response, unsatisfying long-time stability and poor selectivity [15]. In order to overcome these disadvantages, organic–inorganic hybrid sensors are intensively investigated [15–18]. Wu et al. fabricated PANI/SnO_2 hybrid material by a hydrothermal route and found that the PANI/SnO_2 hybrid material could overcome the shortcomings of long response time of PANI and the operation temperature of SnO_2 [15]. Jiang et al. reported that PANI/titanium nanocomposite thin film revealed higher response values, faster response and recover rates to NH_3 than those of a pure PANI film [18].

In order to overcome these disadvantages, such as low sensitivity, poor selectivity, irreversible response and unsatisfying long-time stability, we proposed here a new route to prepare SnO_2–ZnO/PANI composite thick film for sensor applications by using SnO_2–ZnO porous nanosolid as the inorganic part of the sensing material. Firstly, SnO_2–ZnO composite porous nanosolid was prepared by a solvo-thermal hot-press (SHP) process. The porous nanosolid is an intermediate state between nanoparticles and dense nanoceramics, which possesses both high reactivity of nanoparticles and strength of nanoceramics [19]. Previously, we reported that the gas sensor made from ZnO porous nanosolid showed much better sensing performance for several organic

* Corresponding authors at: School of Materials Science and Engineering, University of Jinan, Jinan 250022, PR China. Tel.: +86 531 89736292; fax: +86 531 87974453.
E-mail addresses: mse_xuhy@ujn.edu.cn, hyxu@sdu.edu.cn (H. Xu), mse_caobq@ujn.edu.cn (B. Cao).

0925-4005/$ – see front matter © 2012 Elsevier B.V. All rights reserved.
http://dx.doi.org/10.1016/j.snb.2012.09.060

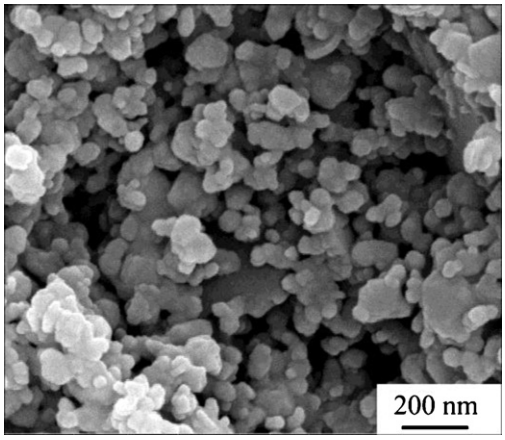

Fig. 1. FESEM image of a SnO_2–ZnO composite porous nanosolid (SZ20).

vapors such as ethanol, acetone and benzens than that built with ZnO nanoparticles [19a]. Similarly, SnO_2–ZnO composite porous nanosolid contains interconnected SnO_2 and ZnO nanoparticles, which forms a framework with numerous pores (Fig. 1). The porous structure is expected to exhibit higher sensor response and quicker response speed. After that, PANI was coated on the SnO_2–ZnO porous thick film by a conventional coating method. Furthermore, the thick film based on the prepared SnO_2–ZnO/PANI composite is difficult to peel off from the substrate. Finally, compared with SnO_2/PANI composite thick film, the sensor response of SnO_2–ZnO/PANI composite thick film to NO_2 gas was much higher. Therefore, it is promising to be used as a kind of NO_2 gas sensor.

2. Experimental

2.1. Preparation of SnO_2–ZnO composite porous nanosolid

The SnO_2–ZnO porous nanosolid was prepared by a solvothermal hot-press (SHP) process, which was conducted in a solvo-thermal hot-press (SHP) autoclave [19a]. The starting materials were SnO_2 nanoparticles, ZnO nanoparticles and dioxane. SnO_2 nanoparticles (with average particle size of 50–70 nm) and ZnO nanoparticles (with average particle size smaller than 20 nm) were purchased from Luoyang Institute of Materials, Henan, China, and used as received. In a typical process, 6 g of SnO_2 and ZnO nanoparticles with different ZnO content (e.g. 0 wt.%, 20 wt.%, 40 wt.%, 60 wt.% and 80 wt.%) was ground with 10 mL dioxane in a high-energy ball mill for 4 h with turning speed of 180 rpm. The resulting paste was mounted into the SHP autoclave. Then the autoclave was applied with a constant pressure of 60 MPa. At the same time, the temperature was raised to 200 °C at a speed of 3 °C min^{-1} and kept at 200 °C for 90 min. Then the autoclave was cooled to room temperature. Thus SnO_2–ZnO composite porous nanosolid was obtained as SZ0, SZ20, SZ40, SZ60 and SZ80 sample, respectively.

2.2. Preparation of PANI

Aniline (purchased, analytical purity) was distilled under reduced pressure and stored at low temperature before usage. Analytical grade hydrochloric acid (HCl, 36–38%), ammonium peroxydisulfate (APS, $(NH_4)_2S_2O_8$) were used directly without further purification.

0.2 g of aniline and 15 mL of anhydrous ethanol were added into a three-neck flask in sequence, sealed, and dispersed by ultrasonic treatment for 5 min. Thereafter the flask was transferred to a thermostatic bath of 0 °C with constant stirring for 15 min, followed by dropwise addition of precooled APS aqueous solution (15 mL, 0.03 M) within ~1 h and maintained at 0 °C for 24 h. The resulting dark blue product was collected by filtration. The precipitates were sequentially washed with distilled water and then anhydrous ethanol several times and finally dried in a vacuum oven at 50 °C for 12 h.

2.3. Preparation of SnO_2–ZnO/PANI composite gas sensors

The thick film gas sensor was prepared as follows. First, 1 g of SZ0 was ground in an agate mortar for 10 min, and 2 mL de-ionized water was added into the agate mortar and ground for another 10 min. Second, the resultant paste was coated on the outer surface of an alumina (Al_2O_3) tube (4.0 mm in length, 1.0 mm in internal diameter and 1.4 mm in external diameter) with a pair of Au electrodes (2.0 mm in distance) attached with Pt lead wires, as shown in Ref. [19a]. Third, the Al_2O_3 tube with SnO_2–ZnO composite was sintered at 650 °C in air for 2 h. Then the gas sensor based on SnO_2–ZnO composite porous nanosolid thick film was obtained.

Then, SnO_2–ZnO porous nanosolid thick film with different ZnO concentration (0 wt.%, 20 wt.%, 40 wt.%, 60 wt.% and 80 wt.%) were prepared and denoted as SZ0, SZ20, SZ40, SZ60 and SZ80, respectively. Three sensors of each kind were fabricated by the same procedure.

Finally, PANI together with NMP (N-methylpyrrolidone) paste with the same content was coated on the outer surface of SnO_2–ZnO porous nanosolid thick film (e.g. SZ0, SZ20, SZ40, SZ60 and SZ80), respectively. After drying at room temperature, SnO_2–ZnO/PANI composite sensors denoted as SZ0-P, SZ20-P, SZ40-P, SZ60-P, and SZ80-P were prepared, respectively. PANI paste was prepared by adding 100 mg of PANI to 1 mL NMP and grounding enough.

For comparison, pure PANI thick film sensors (denoted as P-0) were fabricated. However, the pure PANI film is very loose and tends to peel off from the Al_2O_3 tube. Therefore its sensor response cannot be observed.

2.4. Characterization of the samples

The average pore size, pore volume, and specific surface area of the SnO_2 porous nanosolid were examined by Brunauer–Emmett–Teller (BET) and Barrett–Joyner–Halenda (BJH) methods with a Physisorption Analyzer (Micromeritics, ASAP2020) using a N_2 sorption isotherm. Before being tested, 1.2 g of the porous nanosolid was slightly grounded into large number of particles with average particle size of 200–300 μm. Moreover, it should be heated at 250 °C for 2 h in a vacuum. The Fourier-transform infrared (FTIR) spectroscopy of SnO_2 nanoparticles, ZnO nanoparticles and PANI were measured with a Nicolet NEXUS-670 Fourier-transform infrared (FT-IR) spectroscopy with spectral resolution of 4.00 cm^{-1} and wave number precision of 0.01 cm^{-1}. Scanning electron microscope (SEM) and Field emission scanning electron microscope (FESEM) photographs of the thick film were taken with a Hitachi S-2500 and QUANTA FEG250 scanning electron microscope, respectively. SnO_2 nanoparticles, ZnO nanoparticles and PANI were characterized by X-ray diffraction (XRD). X-ray diffraction patterns were acquired for PANI powders by means of a Rigaku D/max-RB X-ray diffractometer (XRD) equipped with Cu Kα radiation. The θ angle was scanned from 10° to 70°.

2.5. Gas sensing performance

The performance of the sensors was tested with a gas sensor measurement system (WS-30A, Weisheng Electronics, Zhengzhou, China). The gas sensor devices were put into an airproof test box. Prior to the measurement, the sensors were aged at 160 °C for 36 h in air. In order to gain the selectivity of sensors to NO_2 gas, the testing gases are NO_2, NH_3, CO, H_2, and ethanol vapors. The operated

Table 1
Average pore size, pore volume, surface area and porosity of SnO_2–ZnO nanosolid sample SZ0, SZ20, SZ40, SZ60 and SZ80.

Sample	Average pore size (nm)	Pore volume (cm^3/g)	Density (g/cm^3)	Porosity (%)	Specific surface area (m^2/g)
SZ0	22.68	0.032	3.37	10.78	7.31
SZ20	16.02	0.028	2.95	8.26	10.39
SZ40	16.50	0.035	2.62	9.17	10.55
SZ60	22.92	0.016	2.50	4.00	6.04
SZ80	53.91	0.043	2.39	10.28	4.56

electronic circuit is shown in Ref. [19a]. The relationship between the measured voltage values (V_{out}) and sensor resistance values (R_S) is shown as follows:

$$\frac{5 - V_{out}}{R_S} = \frac{V_{out}}{R_L} \quad (1)$$

namely,

$$R_S = \frac{5 - V_{out}}{V_{out}} R_L \quad (2)$$

(here, R_L = 4.7 MΩ)

3. Results and discussion

3.1. Pore size distribution and specific surface area of nanosolid samples

Table 1 shows the average pore size, pore volume and specific surface area of nanosolid sample SZ0, SZ20, SZ40, SZ60 and SZ80. The average pore size decreased firstly and increased lately with the increase of the amount of ZnO. Sample SZ20 has the smallest average pore size of 16.02 nm when the content of ZnO is 20 wt.%. However the changing trend of specific surface area is contrast with that of average pore size. In addition, with the increasing of the content of ZnO, the density of nanosolid samples are smaller and smaller. Moreover, when ZnO was added into the SnO_2, the porosity of nanosolid sample became smaller than that of pure SnO_2 nanosolid sample. It may be caused by the ZnO nanoparticles (with average particle size smaller than 20 nm) filling into the pores built by SnO_2 nanoparticles. Their pore size distributions are shown in Fig. 2. The above results indicate that the pore properties of nanosolid sample obviously change when ZnO nanoparticles are added into SnO_2 nanoparticles.

3.2. FT-IR spectroscopy of SnO_2 nanoparticles, ZnO nanoparticles and PANI

As a nondestructive detection method, Fourier transform infrared spectroscopy (FT-IR) is used to detect the adsorbed impurities in SnO_2 and ZnO nanoparticles. Fig. 3a and b shows the FT-IR spectrum of SnO_2 and ZnO nanoparticles. In these figures, the peak at 3450 cm^{-1} comes from the stretching mode vibrations of —OH, while the peak at 1630 cm^{-1} is attributed to the bending vibrations of adsorbed H_2O molecules. The small peak at 1380 cm^{-1} is due to the bending vibrations of C—H in the methyl which maybe comes from the residues of preparation processes. It indicates that there may be a very small amount of organic residues in the SnO_2 and ZnO nanoparticles. In Fig. 3a, the strong peak at 615 cm^{-1} can be ascribed to the vibration of Sn—O bond in SnO_2 as shown in literature [20–22]. As shown in Fig. 3b, the peak at 471 cm^{-1} can be ascribed to the vibration of Zn—O bond in ZnO [23]. In addition, to verify the composition of PANI, we measured the FT-IR spectrum of the products. As shown in Fig. 3c, the peak around 3732 cm^{-1} is due to the stretching vibration of free N—H. The peak at 1568 cm^{-1} is assigned to the stretching vibration of C=N along with deforming vibration of N—H [24]. The peak at 1488 cm^{-1} corresponds to the stretching vibration of C—C in benzenoid or quinonoid rings [24–29]. The peaks at 1302 and 1246 cm^{-1} are attributed to the stretching vibrations of C—N in benzenoid rings [25–28]. The strongest peak centered at 1135 cm^{-1} is due to the in-plane bending vibration of benzenoid or quinonoid C—H [24,25,29–32]. The peaks around 881–682 cm^{-1} can be assigned to the out-of-plane bending vibrations of benzenoid or quinonoid C—H and N—H [24,29,30]. In addition, the peaks centered at 1568 and 1488 cm^{-1} show a red-shift compared to those of emeraldine base, indicating that the PANI is partially doped [29].

3.3. Crystal structural studies of SnO_2 nanoparticles, ZnO nanoparticles and PANI

The XRD patterns of SnO_2 nanoparticles, ZnO nanoparticles and PANI were shown in Fig. 4. From Fig. 4a, we can find that all diffraction peaks can be indexed to the tetragonal rutile structure of SnO_2. All diffraction peaks in Fig. 4b can be attributed to the hexagonal ZnO structure. Fig. 4c shows the XRD diffraction pattern of PANI. The two diffraction peaks around 20° and 25° for PANI should be assigned to the scattering from the periodicity perpendicular to PANI chains, indicating the crystallization of PANI [33–35]. This is consistent with the results of reported references [36].

3.4. Morphological analysis of SnO_2–ZnO thick films and SnO_2–ZnO/PANI composite thick film

In order to analyze the differences in gas sensing performance between sensors, the surface morphology of SnO_2–ZnO composite

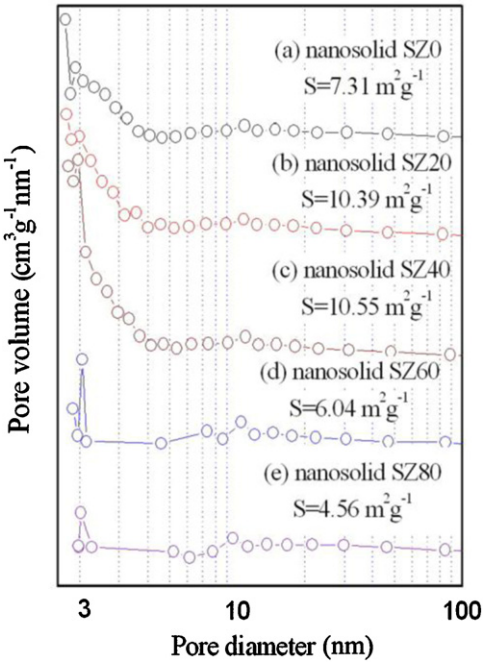

Fig. 2. Pore size distributions of SnO_2–ZnO composite porous nanosolid.

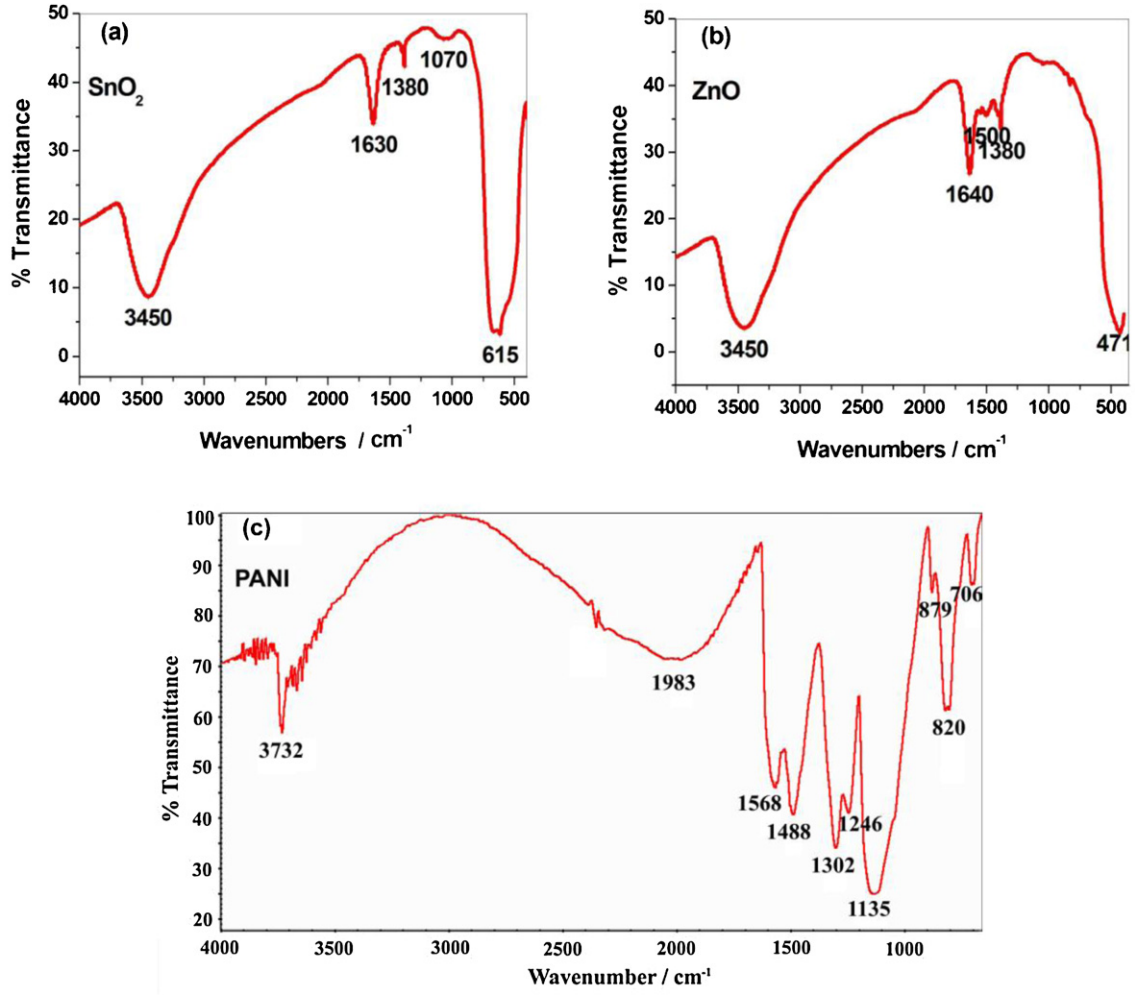

Fig. 3. FT-IR spectra of (a) SnO_2 nanoparticles, (b) ZnO nanoparticles and (c) PANI.

thick films before compounded with PANI were observed through SEM system. It can be seen that, compared with that of SZ0, the particle size of SnO_2–ZnO composite thick film SZ20, SZ40, SZ60 and SZ80 obviously decreased. Moreover, almost all the SnO_2 nanoparticles in SZ0 connect with each other, and much less pores can be observed in SZ0. On the contrary, the growing process of SnO_2 nanoparticles has been suppressed in SZ20 and SZ40, and there are much more pores in these thick films as shown in Fig. 5a–c. As a result, the specific surface of SZ20 and SZ40 is much higher than that of SZ0, and the average pore size of SZ20 and SZ40 is smaller than that of SZ0. However, from Fig. 5d and e, it can be seen that more particles connect with each other when the content of ZnO is higher than 60 wt.%, which leads to the smaller specific and larger pores. These results are agreement with those shown in Table 1.

Fig. 6a shows the surface FESEM image of sample SZ20-P composite thick film. There are a lot of pores (or channels) in PANI thick film, which is greatly beneficial for improving the sensor response. Fig. 6b shows the interface cross-sectional SEM image of sample SZ20-P, which indicates the formation of a diffusion free interface. It is evident that there are many pores on the PANI surface, which would contribute to the short response and recovery times. Due to the porous structure, NO_2 diffusion as well as reaction between gas

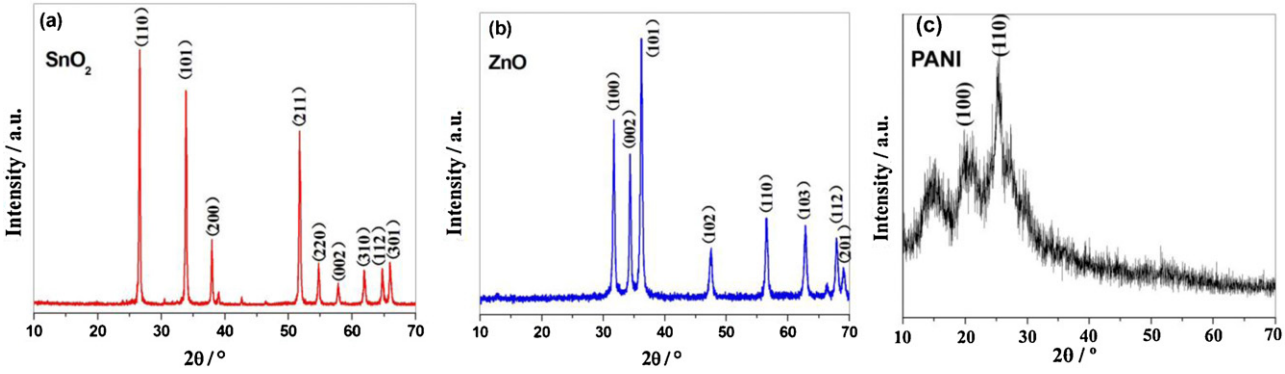

Fig. 4. XRD patterns of (a) SnO_2 nanoparticles, (b) ZnO nanoparticles and (c) PANI.

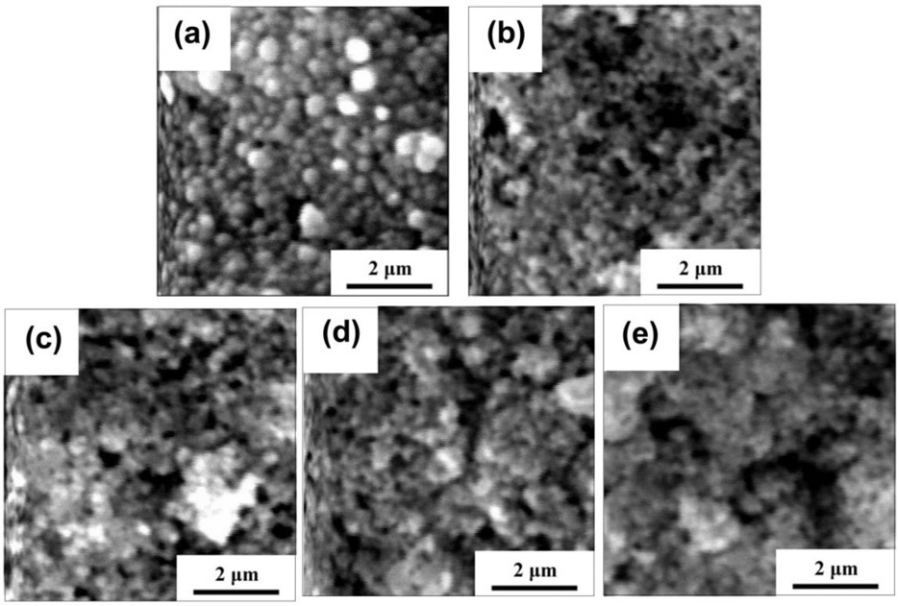

Fig. 5. SEM images of thick film (a) SZ0, (b) SZ20, (c) SZ40, (d) SZ60 and SZ80.

molecules and the interface occurs more easily. In addition, according to our FESEM observation results, all of the structure of PANI film on different SnO_2–ZnO porous nanosolid thick films (including SZ0, SZ20, SZ40, SZ60 and SZ80) are porous and similar.

3.5. Gas sensing properties of SnO_2–ZnO/PANI composite thick film

In order to investigate the effect of ZnO content on the gas sensing properties of SnO_2–ZnO porous nanosolid thick films to NO_2, the sensor response of SZ0, SZ20, SZ40, SZ60 and SZ80 were examined as well. As shown in Fig. 7a, the sensor response of SZ20 and SZ40 to 35 ppm NO_2 is higher than that of SZ0, SZ60 and SZ80 when the working temperature is higher than 180 °C.

In order to improve the gas sensing properties, we compounded the SnO_2–ZnO porous nanosolid thick films with PANI in our experiments, and we found that the sensor response of composite thick films became much stronger. Fig. 7b shows the relationship between working temperature and sensor response of SnO_2–ZnO/PANI composite thick film sensors SZ0-P, SZ20-P, SZ40-P, SZ60-P, and SZ80-P to 35 ppm NO_2. It can be seen that the content of ZnO has large effect on the response of SnO_2–ZnO/PANI composite thick film to NO_2. Sensor SZ20-P has the highest response when the working temperature was higher than 160 °C. Moreover, the sensor response to 35 ppm NO_2 increases from 40 to 180 °C and decreases after 180 °C. SZ20-P has the highest sensor response of 368.9 at 180 °C. Compared with that of SZ20 as shown in Fig. 7a, the sensor response of SZ20-P to 35 ppm NO_2 is much higher at 180 °C. Those indicate that compounding with PANI can greatly improve the sensor response of the SnO_2–ZnO porous nanosolid thick films.

It should be noted that an important point in a sensor system is the selectivity. The sensor responses of SZ20-P to different gases are compared in Fig. 8, showing that the sensor exhibits the highest response to NO_2. It indicates that SnO_2–ZnO/PANI composite thick film SZ20-P exhibits high selectivity to NO_2 gas among the different gases.

Fig. 9 shows the dynamic response of both sensors toward NO_2 gas in varying concentration. The measurements were carried out at 180 °C. Notably, the voltage value of both sensors decreases marginally after NO_2 removal, indicating that small amounts of NO_2 molecules fail to desorb from the surface, which might have little influence on the gas sensing properties of the sensors. In addition, with the increasing of concentration of NO_2, the change of voltage value of sensor SZ20-P are much greater than that of sensor SZ20, indicating a better sensor response characteristic.

There are two competitive mechanisms of electronic properties in the SnO_2–ZnO/PANI composite thick film. ZnO and SnO_2 are n-type semiconductors, in which adsorbed oxygen reacts with the test gas, releasing electrons in to the conduction band by which the conductivity increases [37]. While PANI films are normally of p-type semiconductor. This is due to the fact that during the polymerization process of aniline, acids (such as HCl) are used, which

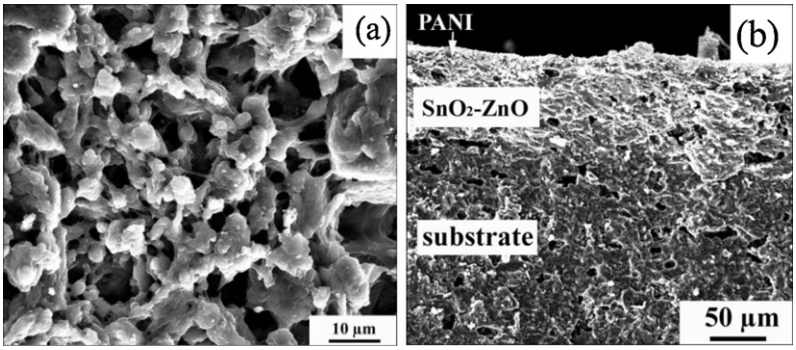

Fig. 6. FESEM images of (a) surface and (b) an interface cross-section of a SZ20-P.

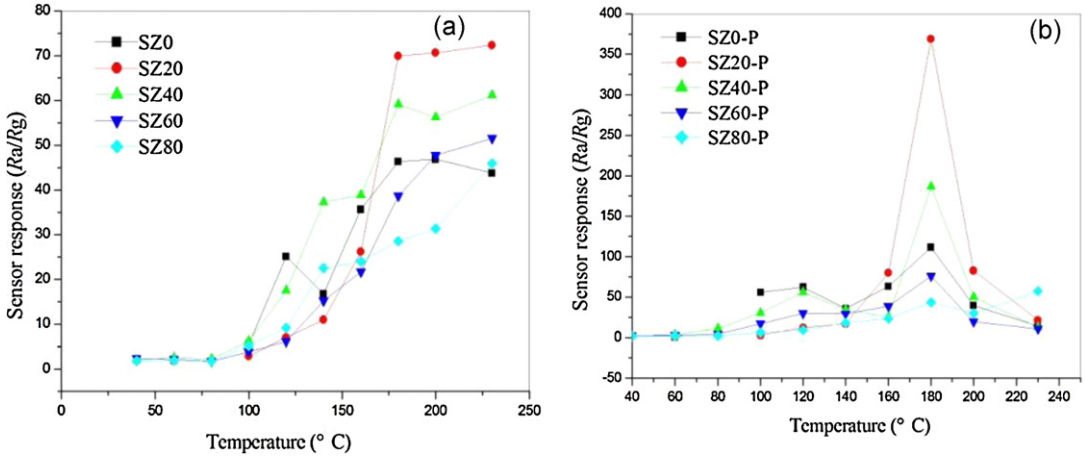

Fig. 7. Sensor response of (a) SZ0, SZ20, SZ40, SZ60, SZ80 and (b) SZ0-P, SZ20-P, SZ40-P, SZ60-P, SZ80-P to 35 ppm NO_2 at different working temperatures.

acts as dopant for PANI molecules, and usually bound with the central N atom of aniline (monomer) molecule, like H^+—N—Cl^- (other bonds on sides of N atom are left here for want of clarity, and more details are provided in literature, see Fig. 4 of Ref. [38]). In equilibrium at room temperature, the positive charge of bonded hydrogen shifts on N atom, making the structure looks like H—N^+—Cl^-. While the negative charge on Cl^- is retained with it and remains localized, the positive charge on nitrogen becomes mobile charge in PANI matrix, via its other bonds, making the PANI as a p-type semiconductor [38,39]. In our experiments, when exposed to NO_2 gas, SnO_2–ZnO/PANI composite thick films exhibit the properties of n-type semiconductors; that is, the resistance of n-type semiconductor increases when exposed to oxidizing gases. It suggests that the sensing mechanism of SnO_2–ZnO/PANI composite is governed by SnO_2–ZnO porous nanosolid thick film. It can be explained that there are many p–n heterojunctions at the interface between SnO_2–ZnO and PANI. Moreover, a positively charged depletion layer on the surface of SnO_2–ZnO could be formed owing to interparticle electron migration from SnO_2–ZnO to PANI at the p–n heterojunctions, lowering the activation energy and enthalpy of physisorption for gas with good electron-donating characteristics [15,37]. Because SnO_2–ZnO porous nanosolid thick film connected with two gold electrodes on the Al_2O_3 tube, the electron transmission is governed by SnO_2–ZnO. Moreover, the ZnO content and pore properties of SnO_2–ZnO nanosolid thick film will affect the electron transmission and sensing properties. In addition, large specific area and small pores will be beneficial for the improvement of sensing performance of thick film. Compared with that of the other four sensors, more NO_2 gas molecules can be adsorbed and diffuse into the inner part of SnO_2–ZnO composite thick film SZ20 because of its larger specific surface and smaller pores as shown in Table 1 and Fig. 5. Moreover, PANI will be more easily compounded with those thick films with larger specific surface and smaller pores. This phenomenon should be the main reason for the significant improvement of sensing performance of the composite gas sensor SZ20-P.

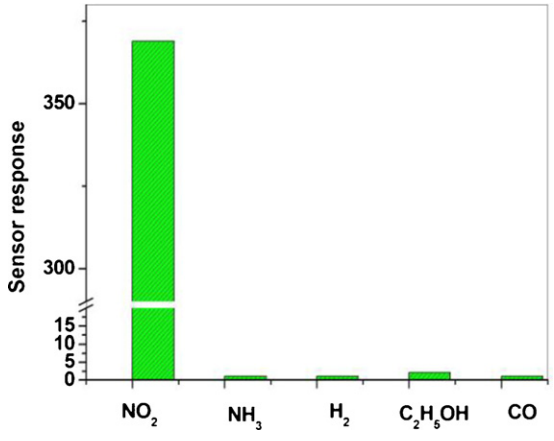

Fig. 8. Responses of sensor SZ20-P at 180 °C to NO_2, NH_3, H_2, C_2H_5OH and CO, the concentration of NO_2 and NH_3 is 10 ppm, and that of H_2, C_2H_5OH and CO is 1000 ppm.

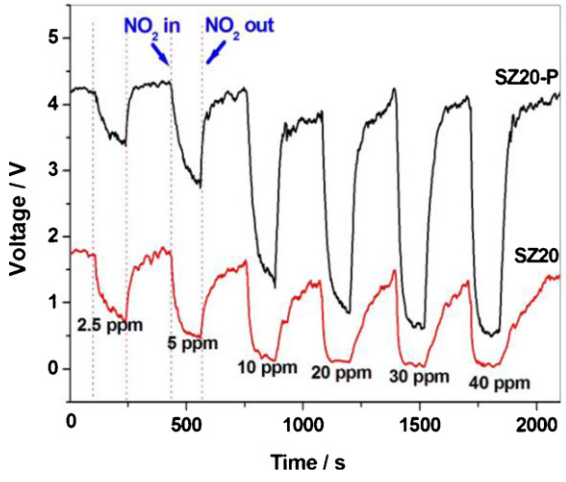

Fig. 9. Dynamic response of sensors to different concentrations of NO_2 at 180 °C.

In order to examine the stability of composite sensors to NO_2 over a long working period, both the performance of sensor SZ20 and SZ20-P were continuously monitored for 22 min. During this process, 35 ppm NO_2 was repeatedly introduced into the chamber and then evacuated. Fig. 10 shows the voltage signal versus time curves at 180 °C. When NO_2 was introduced into the test chamber, the voltage of SZ20-P decreased within a few seconds. When NO_2 was evacuated from the chamber, the voltage recovered to its original value very quickly. The response/recovery time is another important parameter used for characterizing a sensor. Generally, the response time is defined as the duration within which the signal voltage reaches 90% of its maximum value when gas is introduced into the chamber, and the recovery time is the interval of which the voltage decreases by 90% of its maximum value. According to this definition, the response time of SZ20 and SZ20-P to NO_2 is estimated to be about 28 and 9 s, respectively, while its recovery

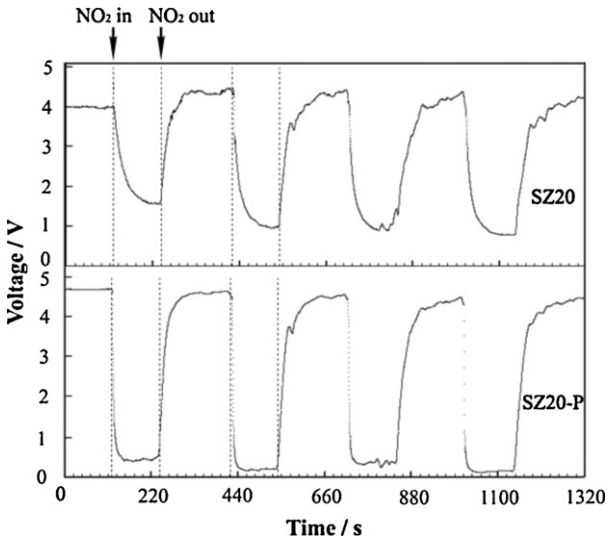

Fig. 10. Sensing performances of sensor SZ20 and SZ20-P at 180 °C over a long working period. The target gas is NO_2 with a concentration of 35 ppm.

time is 20 and 27 s, respectively. In addition, the response curve in Fig. 10 can be repeatedly obtained by injecting and evacuating NO_2. To the best of our knowledge, no PANI, or SnO_2/PANI composite synthesized by other methods exhibit more rapid response and recovery speed to NO_2 gas reported in literature. For example, the response and recovery time of SnO_2 thin film to 50 ppm NO_2 was several and tens of minutes at 140 °C, respectively [38]. The next example is that the response time (when $R/R_0 = 10$) of PANI nanofiber sensor to 50 ppm NO_2 is 173 s at room temperature [39]. The rapid response and recovery speed of our SnO_2–ZnO/PANI composite thick film may be due to the porous structure of SnO_2–ZnO porous nanosolid and PANI thick film as shown in Figs. 5 and 6. Due to the porous structure, NO_2 diffusion as well as reaction between gas molecules and the interface occurs more easily. Our experimental results indicate that the SnO_2–ZnO/PANI composite sensor with rapid response and recovery speed are quite stable and would be useful for recyclable NO_2 sensors.

The stability of the sensor SZ20-P and SZ20 was also investigated after 7 months. As shown in Fig. 11, the sensors both do not lose its fast response and recovery characteristics to NO_2 compared with its original performances shown in Fig. 10. However, as shown in Fig. 11, sensor SZ20 seems to lose its original stability in the process

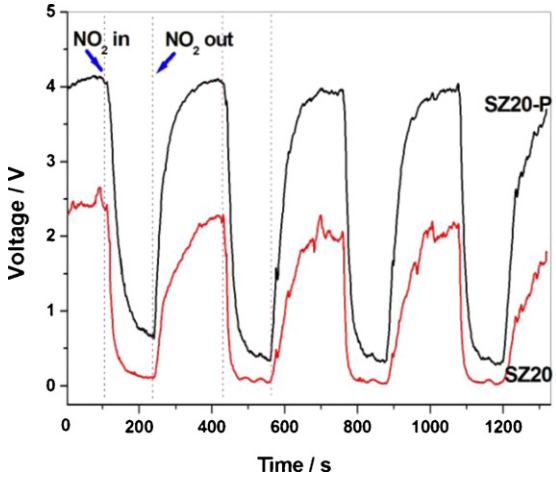

Fig. 11. Sensing performances of sensor SZ20 and SZ20-P at 180 °C over a long working period after 7 months. The target gas is NO_2 with a concentration of 35 ppm.

of NO_2 desorption. In addition, the voltage value of sensor SZ20 in air is much lower compared with its original one shown in Fig. 10. Those indicate that the sensor SZ20-P exhibits a better stability.

4. Conclusions

In summary, an inorganic/organic SnO_2–ZnO/PANI composite sensor was prepared by using a novel SnO_2–ZnO porous nanosolid and PANI. The composite sensor fabricated can overcome the shortcomings of long response time of PANI and the high working temperature of SnO_2. It has high selectivity, high sensor response, short response and recovery time, low optimum working temperature (180 °C) and high stability to low concentration NO_2 gas. The response time was only a few seconds, and the recovery time was a few tens of seconds.

To our knowledge, most of semiconductor metal oxide (such as SnO_2, ZnO and Fe_2O_3) and their compound metal oxide porous nanosolid can be prepared by the solvothermal hot-press (SHP) process. Furthermore, the porous nanosolid can be well compounded with organic materials, therefore this novel method possesses a wide versatility, which makes it possible to develop other new kinds of chemical gas sensors and micro-cavity optoelectronic devices.

Acknowledgments

This work is supported by National Natural Science Foundation of China (NSFC, No. 60906008), the Foundation for Excellent Middle-aged or Young Scientists from Shandong Province under Grant (Nos. BS2010CL007 and BS2012CL003) and the Open Research Project (No. KF0808) from State Key Laboratory of Crystal Material (Shandong University).

References

[1] B.T. Marquis, J.F. Vetelino, A semiconducting metal oxide sensor array for the detection of NO_x and NH_3, Sensors and Actuators B 77 (2001) 100–110.
[2] J. Brunet, V.P. Gracia, A. Pauly, C. Varenne, B. Lauron, An optimised gas sensor microsystem for accurate and real-time measurement of nitrogen dioxide at ppb level, Sensors and Actuators B 134 (2008) 632–639.
[3] Z. Ling, C. Leach, The effect of relative humidity on the NO_2 sensitivity of a SnO_2/WO_3 heterojunction gas sensor, Sensors and Actuators B 102 (2004) 102–106.
[4] A.A. Firooz, T. Hyodo, A.R. Mahjoub, A.A. Khodadadi, Y. Shimizu, Synthesis and gas-sensing properties of nano- and meso-porous MoO_3-doped SnO_2, Sensors and Actuators B 147 (2010) 554–560.
[5] H.Y. Xu, Y.T. Song, D.L. Cui, Effects of SnO_2 doping on the performance of ZnO porous thick film gas sensors, Materials Science Forum 687 (2011) 55–60.
[6] H.Y. Xu, X.Q. Chen, L.Z. Fang, B.Q. Cao, Preparation and characterization of cerium-doped tin oxide gas sensors, Advances in Materials Research 306–307 (2011) 1450–1455.
[7] D.W. Hatechett, M. Josowicz, Composites of intrinsically conducting polymers as sensing nanomaterials, Chemical Reviews 108 (2008) 746–769.
[8] U. Lange, N.V. Roznyatovskaya, V.M. Mirsky, Conducting polymers in chemical sensors and arrays, Analytica Chimica Acta 614 (2008) 1–26.
[9] H. Bai, G.Q. Shi, Gas sensors based on conducting polymers, Sensors 7 (2007) 267–307.
[10] M.I. Newton, T.K.H. Starke, M.R. Willis, G. McHale, NO_2 detection at room temperature with copper phthalocyanine thin film devices, Sensors and Actuators B 67 (2000) 307–311.
[11] Y.L. Lee, C.H. Chang, NO_2 sensing characteristics of copper phthalocyanine films: effects of low temperature annealing and doping time, Sensors and Actuators B 119 (2006) 174–179.
[12] C. Park, D.H. Yun, S.T. Kim, Y.W. Park, Enhancement of the NO_2-sensing capability of copper phthalocyanine by measuring the relative resistance change, Sensors and Actuators B 30 (1996) 23–27.
[13] N.G. Deshpande, Y.G. Gudage, R. Sharma, J.C. Vyas, J.B. Kim, Y.P. Lee, Studies on tin oxide-intercalated polyaniline nanocomposite for ammonia gas sensing applications, Sensors and Actuators B 138 (2009) 76–84.
[14] A.A. Athawale, S.V. Bhagwat, P.P. Katre, Nanocomposite of Pd–polyaniline as a selective methanol sensor, Sensors and Actuators B 114 (2006) 263–267.
[15] L.N. Geng, Y.Q. Zhao, X.L. Huang, S.R. Wang, S.M. Zhang, S.H. Wu, Characterization and gas sensitivity study of polyaniline/SnO_2 hybrid material prepared by hydrothermal route, Sensors and Actuators B 120 (2007) 568–572.

[16] A. Choudhury, Polyaniline/silver nanocomposites: dielectric properties and ethanol vapour sensitivity, Sensors and Actuators B 138 (2009) 318–325.
[17] M.L. Singla, S. Awasthi, A. Srivastava, Humidity sensing; using polyaniline/Mn_3O_4 composite doped with organic/inorganic acids, Sensors and Actuators B 127 (2007) 580–585.
[18] H.L. Tai, Y.D. Jiang, G.Z. Xie, J.S. Yu, X. Chen, Fabrication and gas sensitivity of polyaniline–titanium dioxide nanocomposite thin film, Sensors and Actuators B 125 (2007) 644–650.
[19] (a) H.Y. Xu, X.L. Liu, D.L. Cui, M. Li, M.H. Jiang, A novel method for improving the performance of ZnO gas sensors, Sensors and Actuators B 114 (2006) 301–307; (b) H. Xu, X. Liu, M. Li, Z. Chen, D. Cui, M. Jiang, X. Meng, L. Yu, C. Wang, Preparation and characterization of TiO_2 bulk porous nanosolids, Materials Letters 59 (2005) 1962–1966;
(c) X. Liu, L. Yu, H. Xu, M. Li, C. Wang, M. Jiang, D. Cui, Degradation of RhB catalyzed by TiO_2 bulk porous nanosolids, Acta Chimica Sinica 62 (2004) 2398–2402.
[20] K. Dutta, S.K. De, Optical and nonlinear electrical properties of SnO_2–polyaniline nanocomposites, Materials Letters 61 (2007) 4967–4971.
[21] G. Zhong, M. Liu, Preparation of nanostructured tin oxide using a sol–gel process based on tin tetrachloride and ethylene glycol, Journal of Materials Science 34 (1999) 3213–3219.
[22] S. Monredon, A. Cellot, F. Ribot, C. Sanchez, L. Armelao, L. Gueneau, L. Delattre, Synthesis and characterization of crystalline tin oxide nanoparticles, Journal of Materials Chemistry 12 (2002) 2396–2400.
[23] Y.Y. Hong, S.Z. Zhang, G.Q. Di, H.Z. Li, Y. Zheng, J. Ding, D.G. Wei, Preparation, characterization and application of Fe_3O_4/ZnO core/shell magnetic nanoparticles, Materials Research Bulletin 43 (2008) 2457–2468.
[24] L.G. Gai, G.J. Du, Z.Y. Zuo, Y.M. Wang, D. Liu, H. Liu, Controlled synthesis of hydrogen titanate–polyaniline composite nanowires and their resistance-temperature characteristics, Journal of Physical Chemistry C 113 (2009) 7610–7615.
[25] C.Q. Bian, Y.J. Yu, G. Xue, Synthesis of conducting polyaniline/TiO_2 composite nanofibres by one-step in situ polymerization method, Journal of Applied Polymer Science 104 (2007) 21–26.
[26] H. Liu, J.Y. Wang, X.B. Hu, R. Boughton, S.R. Zhao, Q. Li, M.H. Jiang, Structure electronic transport properties of polyaniline/$NaFe_4P_{12}$ composite, Chemical Physics Letters 352 (2002) 185–190.
[27] N. Parvatikar, S. Jain, C.M. Kanamadi, B.K. Chougule, S.V. Bhoraskar, M.V.A. Prasad, Humidity sensing and electrical properties of polyaniline/cobalt oxide composites, Journal of Applied Polymer Science 103 (2007) 653–658.
[28] Y. Qiu, L. Gao, Novel polyaniline/titanium nitride nanocomposite: controllable structures and electrical/electrochemical properties, Journal of Physical Chemistry B 109 (2005) 19732–19740.
[29] L.X. Zhang, P. Liu, Z.X. Su, Preparation of PANI–TiO_2 nanocomposites and their solid-phase photocatalytic degradation, Polymer Degradation and Stability 91 (2006) 2213–2219.
[30] H. Liu, X.B. Hu, J.Y. Wang, R.I. Boughton, Structure, conductivity, and thermopower of crystalline polyaniline synthesized by the ultrasonic irradiation polymerization method, Macromolecules 35 (2002) 9414–9419.
[31] B.B. Rao, Zinc oxide ceramic semi-conductor gas sensor for ethanol vapor, Materials Chemistry and Physics 64 (2000) 62–65.
[32] A.L. Kukla, Y.M. Shirshov, S.A. Piletsky, Ammonia sensors based on sensitive polyaniline films, Sensors and Actuators B 37 (1996) 135–140.
[33] C. Bian, G. Xue, Nanocomposites based on rutile-TiO_2 and polyaniline, Materials Letters 61 (2007) 1299–1302.
[34] S. Jiang, J.Y. Chen, J. Tang, E. Jin, L.R. Kong, W.J. Zhang, C. Wang, Au nanoparticles-functionalized two-dimensional patterned conducting PANI nanobowl monolayer for gas sensor, Sensors and Actuators B 140 (2009) 520–524.
[35] G.Z. Xie, P. Sun, X.L. Yan, X.S. Du, Y.D. Jiang, Fabrication of methane gas sensor by layer-by-layer self-assembly of polyaniline/PdO ultra thin films on quartz crystal microbalance, Sensors and Actuators B 145 (2010) 373–377.
[36] J. Huang, T.L. Yang, Y.F. Kang, Y. Wang, S.R. Wang, Gas sensing performance of polyaniline/ZnO organic–inorganic hybrids for detecting VOCs at low temperature, Journal of Natural Gas Chemistry 20 (2011) 515–519.
[37] P.J. Benjamin, E. Phillip, J.E. Richard, L.H. Colin, M.R. Norman, Novel composite organic–inorganic semiconductor sensors for the quantitative detection of target organic vapours, Journal of Materials Chemistry 6 (1996) 289–294.
[38] A. Sharma, M. Tomar, V. Gupta, SnO_2 thin film sensor with enhanced response for NO_2 gas at lower temperatures, Sensors and Actuators B 156 (2011) 743–752.
[39] X.B. Yan, Z.J. Han, Y. Yang, B.K. Tay, NO_2 gas sensing with polyaniline nanofibers synthesized by a facile aqueous/organic interfacial polymerization, Sensors and Actuators B 123 (2007) 107–113.

Biographies

Hongyan Xu received her Ph.D. degree from State Key Lab of Crystal Materials, Shandong University in 2006. Now she is an Associate Professor at School of Materials Science and Engineering, University of Jinan. Her main research interests are the synthesis and fabrication of semiconductor nano-materials and high performance conductive polymer composite chemical gas sensors.

Xingqiao Chen obtained his B.S. degree from the College of Electrical and Information Engineering, Hunan University of Technology in 2001. He is currently an Engineer in Shandong Swan Cotton Industrial Machinery Stock Co., Ltd. His research interests are the fabrication of semi-conductive material gas sensors.

Jun Zhang received his Ph.D. degree from the Department of Chemistry, Nankai University in 2011. Now he is working at School of Materials Science and Engineering, University of Jinan. His research is focused on gas sensing materials.

Jieqiang Wang graduated from Northeastern University in 1999 and received his Ph.D. degree. Now he is a Professor at School of Materials Science and Engineering, University of Jinan. His main research interests are the synthesis and fabrication of semiconductor nano-materials.

Bingqiang Cao received the Ph.D. degree from the Institute of Solid State Physics, Chinese Academy of Sciences (CAS) in 2006. After that, he worked as a postdoctoral researcher at University of Leipzig from September 2006 to August 2008, and then as a JSPS fellow at Kyushu University from August 2008 to July 2009. He then joined the faculty of University of Jinan in China as a Principle Investigator and Oversea Taishan Scholar endowed professor. His research is focused on nanostructures, heterostructures, thin films, and transparent optoelectrical devices based on inorganic semiconductors.

Deliang Cui graduated from Jilin University in 1989 and received his Master degree. From 1989 to 1992, he was employed by Tianjin Institute of Technology. In 1995, he received his Ph.D. degree from Jilin University. Now he is a Professor at State Key Lab of Crystal Materials, Shandong University, and his main research interest is the preparation of semiconductor nano-materials and the fabrication of chemical sensors.